Nano Energy (2015) 15, 235–243

Available online at www.sciencedirect.com

ScienceDirect

journal homepage: www.elsevier.com/locate/nanoenergy

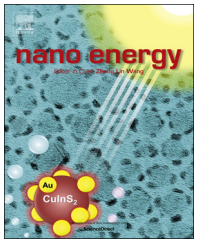

RAPID COMMUNICATION

Free-standing boron and oxygen co-doped carbon nanofiber films for large volumetric capacitance and high rate capability supercapacitors

Zi-You Yu[a], Li-Feng Chen[a], Lu-Ting Song[a], Yan-Wu Zhu[b], Heng-Xing Ji[b], Shu-Hong Yu[a,*]

[a]*Division of Nanomaterials and Chemistry, Hefei National Laboratory for Physical Sciences at Microscale, Collaborative Innovation Center of Suzhou Nano Science and Technology, Department of Chemistry, University of Science and Technology of China, Hefei, Anhui 230026, PR China*
[b]*Department of Materials Science and Engineering and CAS Laboratory of Materials for Energy Conversion, University of Science and Technology of China, PR China*

Received 19 March 2015; received in revised form 16 April 2015; accepted 21 April 2015
Available online 1 May 2015

KEYWORDS
Carbon nanofiber film;
Heteroatom doping;
Volumetric capacitance;
Supercapacitor

Abstract
Carbon-based materials are the most common and important supercapacitor electrode materials, and have been attracting much attention for researchers. Although much work has focused on increasing the gravimetric capacitance of carbon materials, it is highly needed to obtain high volumetric capacitance for real compact device application. Therefore, a finely tuned carbon material structure with both optimal gravimetric and volumetric capacitances has been becoming a considerable challenge. In this work, we synthesized free-standing boron and oxygen co-doped carbon nanofiber (BO-CNF) films for the first time. Both high gravimetric and volumetric capacitances (192.8 F g^{-1} and 179.3 F cm^{-3} at 1 A g^{-1}) can be obtained by an optimized design with regulating the heteroatom content and packing density. Meanwhile, the BO-CNF film with a relatively high packing density exhibits an excellent rate capability (78.5% capacitance retention from 1 to 100 A g^{-1}), which is due to the formation of continuous electrolyte ion diffusion network as well as good electrical conductivity. Such BO-CNF film provides an excellent platform for depositing polyaniline active materials and the boron dopant can be recycled to reduce the cost for the possibly scalable application.

*Corresponding author.
E-mail address: shyu@ustc.edu.cn (S.-H. Yu).

http://dx.doi.org/10.1016/j.nanoen.2015.04.017
2211-2855/

Introduction

Supercapacitors have been attracting much attention in electrical energy storage devices, mainly owing to their more outstanding power density and longer cycle life than that of lithium-ion batteries [1,2]. Carbon-based materials are the most common and important electrode materials, and have been used in more than 80% of the commercially available supercapacitors as a result of their low cost, excellent conductivity, and ultrahigh power density [3-5]. Nevertheless, the capacitance values of carbon materials are generally low, leading to a limited energy density [6,7].

According to the geometric capacitor model that $C=A\varepsilon_0\varepsilon/d$ (where A is the total area of the electrode/electrolyte interface, d is the charge separate distance, ε_0 and ε are vacuum dielectric constant and the relative dielectric constant of electrolyte, respectively), a straight forward way to increase the gravimetric capacitance is to using carbon materials with high specific surface area prepared by, for example, activation in water vapor, KOH, or CO_2 to enhance the gravimetric capacitance [1,8,9]. However, the activated carbon materials suffer from some disadvantages: (i) the activation process generally results in a low carbon yield and needs high equipment consume [10]; (ii) a highly porous carbon structure breaks electron conductive pathways, thus decreasing the electrical conductivity and power output [11,12]; (iii) the powder nature of these carbon materials needs the addition of polymer binder and conductive agent, which undergoes a complex process and unavoidably causes an adverse effect on the energy density [13]. Nevertheless, the most important issue lying in porous carbon based supercapacitor electrodes is the low packing density (usually less than 0.5 g cm^{-3}) of the carbon electrodes with the low volumetric capacitance, which is difficult to achieve a compact electrode design for real device application and leads to practically lower gravimetric performance as well [4,14-20]. Therefore, it is a trade-off between the gravimetric capacitance and the volumetric capacitance since a loosely porous structure favors high gravimetric capacitance; yet a relatively compacted structure is necessary for improving volumetric capacitance.

With respect to the above considerations, a finely tuned carbon material structure with both optimal gravimetric and volumetric capacitance has become an open question in supercapacitor research, and fabricating free-standing and highly packed film electrodes has been a promising method to meet these requirements [16,21-25]. Recently, Li and coworkers have made great progress and developed liquid electrolyte-mediated chemically converted graphene films with a relatively high gravimetric capacitance of 170.6 F g^{-1} at 1 A g^{-1} at a packing density of 1.33 g cm^{-3} [22], while this strategy may be more suitable for graphene film materials. A universal approach to enhance gravimetric capacitance without activation process is to incorporate pseudocapacitive properties by introducing heteroatoms (e.g. N, B, O etc.) into carbon structures [26-34]. Although heteroatom-doped carbon materials have exhibited excellent enhancement in the capacitive performance [27,29,32,33], their volumetric capacitance and rate capability are still unsatisfying and further improvements are needed.

Recently, in our group, a hydrothermal carbonization method by using Te nanowires as the template and glucose as the carbon source has been developed to synthesize carbonaceous nanofibers and hydrogel/aerogel with large volume (up to 12 L) [35,36]. Herein, we adopted our as-obtained carbonaceous nanofibers as the precursor to prepare high packing density boron and oxygen co-doped carbon nanofiber (BO-CNF) films for the first time. With the increase of heteroatom content, the gravimetric capacitance is increased from 76.5 to 225.9 F g^{-1} at 1 A g^{-1} while the packing density is decreased. We found that the carefully balanced porous microstructure created during the doping process, pseudocapacitance contributed from the dopants, and the packing density are the keys to simultaneously achieve a gravimetric capacitance of 192.8 F g^{-1} and a volumetric capacitance of 179.3 F cm^{-3} at 1 A g^{-1} with specific surface area of 594.6 m^2 g^{-1} and packing density of 0.93 g cm^{-3}. Exceptionally, owing to the formation of continuous electrolyte ion diffusion network as well as good electrical conductivity, the BO-CNF film delivers a remarkable rate capability (78.5% capacitance retention with charge/discharge current densities increasing from 1 to 100 A g^{-1}). We also show that the BO-CNF film is an optimal platform for depositing polyaniline nanoparticles to obtain a higher volumetric capacitance (359.1 F cm^{-3} at 1 A g^{-1}). Meanwhile, it is interesting to find that the boron source used in our synthesis process can be recycled with a recovery ratio of about 50%, which is beneficial to industrial application.

Materials and methods

All of the chemicals were analytical grade and commercially available from Shanghai Chemical Reagent Co. Ltd. and used as received without any further purification.

Preparation of BO-CNF films

The carbonaceous nanofibers were prepared according to the previous study in our team [35,36], and were dispersed in ethanol with a concentration of about 6 mg mL^{-1}. Different masses of boric acid (0, 10, 20, 40, and 80 mg) were dissolved into 1 mL ethanol, followed by addition of 4 mL of the above carbonaceous nanofibers with vigorous stirring to form a homogeneous suspension. The suspension was cast onto a round Teflon substrate (5 cm in diameter), and a free-standing film could be obtained after drying at ambient temperature for about 12 h. The free-standing film was then annealed at 800 °C for 2 h under Ar atmosphere. Finally, the carbonized film was washed in deionized water of 100 °C to remove the boric oxide. The corresponding films with 0, 10, 20, 40, and 80 mg of initial boric acid were denoted as CNF and BO-CNF-1, 2, 3, 4 films, respectively.

Preparation of BO-CNF@PANI films

A piece of BO-CNF-2 film was immersed in 20 mL of 1.0 M $HClO_4$ solution with 0.1 mL of aniline monomer and 0.06 g of $(NH_4)_2S_2O_8$ (APS, the oxidant) was dissolved in 15 mL of 1.0 M $HClO_4$ solution. The two solutions were precooled at 0-5 °C for 2 h. Then, the APS solution was added to aniline monomer solution dropwise with continuous shaking and the mixture was stored at 0-5 °C for polymerization. After reaction, the composite film was rinsed with ethanol and deionized water, and dried at 60 °C. BO-CNF-2@PANI-2 h,

4 h, 6 h films were prepared at different polymerization times of 2 h, 4 h, and 6 h, respectively. The weight fraction of PANI nanoparticles in BO-CNF-2@PANI-2 h, 4 h, 6 h films were 10.6 wt%, 28.2 wt%, and 33.5 wt%, which was obtained by weighing the film before and after polymerization. From our results in Figures S10 and S11, the BO-CNF-2@PANI-4 h film showed the best electrochemical performances and the best reaction time was 4 h. The CNF@PANI-4 h film was also prepared with a weight fraction of PANI of 26.8 wt%.

Recycling of boron source

The BO-CNF film after carbonization was boiled in a sealed beaker with 20 mL deionized water at 100 °C for 10 h to ensure the reaction between boric oxide and water completely. After the sealed beaker was cooled down, the boric acid aqueous solution was poured into the Teflon substrate (the detaching of boric acid is much easier from Teflon than glass substrate). Thereafter, the Teflon substrate was moved to a vacuum oven at 60 °C until the deionized water evaporates completely and boric acid powder was obtained, which could be used for recycling of BO-CNF film. We can obtain about 13.5 mg carbon film from 24 mg carbonaceous nanofibers, leading to about 56% yield for carbon. For the yield of boric acid dopant, we obtained the weight ratio of B atom with 0.96, 1.40, 1.73, and 1.93 wt% for BO-CNF-1, 2, 3, 4 samples from the result of atom ratio (Table 1). Thus, the B atom masses of BO-CNF-1, 2, 3, 4 samples incorporated in carbon skeleton were 0.13, 0.19, 0.23, and 0.26 mg, respectively. Based on the initial mass of 10, 20, 40, and 80 mg boric acid dopant for BO-CNF-1, 2, 3, 4 samples, the yields of dopant were 7.4%, 5.4%, 3.3%, and 1.9%, respectively. Such low doping ratio verifies that it is highly essential to recycle boron source for the possibly commercial application.

Characterizations

Scanning electron microscopy (SEM) images were carried out on a field emission scanning electron microanalyzer (Zeiss Supra 40) at an acceleration voltage of 5 kV. For the thickness evaluation of each film, we prepared three cross-sectional SEM samples from three independent films and the thickness was obtained by averaging the different SEM samples. X-ray photoelectron spectra (XPS) were done on an X-ray photoelectron spectrometer (ESCALab MKII) with an excitation source of Mg Kα radiation (1253.6 eV). Raman scattering spectra was conducted on a Renishaw System 2000 spectrometer using the 514.5 nm line of Ar^+ for excitation. The powder X-ray diffraction (XRD) studies were carried on a Philips X'Pert Pro Super X-ray diffractometer equipped with graphite monochromatized Cu Kα radiation (λ=1.541841 Å). N_2 (77 K) and CO_2 (273 K) sorption analysis was determined with an ASAP 2020 accelerated surface area and a porosimetry instrument (Micromeritics). Sheet resistance was obtained from a four-probe conductivity test (ST-21, Guangzhou Four-Point Probes Technology).

Electrochemical measurement

Our supercapacitor cells were assembled in a two-electrode system using 1.0 M H_2SO_4 aqueous solution as electrolyte and platinum plate as current collector. The sizes of all films were about 1.0 cm × 1.0 cm and the areal mass densities of CNF and BO-CNF films were 1.3-1.5 mg cm^{-2}. The electrochemical performances were evaluated by the cyclic voltammetry (CV) at different scan rates and galvanostatic charge-discharge at different current densities in a CHI 760D electrochemical workstation. Electrochemical impedance spectroscopy (EIS) was performed under a frequency range of 10 mHz to 100 kHz with an alternate current amplitude of 5 mV.

The gravimetric and volumetric capacitances of film electrodes were calculated from the galvanostatic discharge curves using the following equations [22]:

$$C_s = \frac{2I_s \times \Delta t}{m \times \Delta U} \quad (1)$$

$$C_v = C_s \times \rho \quad (2)$$

where C_s (F g^{-1}) and C_v (F cm^{-3}) correspond to gravimetric and volumetric capacitances of films, m (g) and ρ (g cm^{-3}) refer to the mass and packing density of single electrode, I_s (A) is the constant current, Δt (s) is the discharge time, and ΔU (V) is the potential window.

Energy density (E, W h L^{-1}) and average power density (P_{av}, W L^{-1}) of supercapacitor cells were obtained from the following equation:

$$E = C_v \times (\Delta U)^2/8 \quad (3)$$

$$P_{av} = \frac{E}{\Delta t} \quad (4)$$

The maximum power density (P_{max}, W L^{-1}) was calculated using the formula:

$$P_{max} = \frac{(\Delta U)^2 \times \rho}{4(2m) \times R_s} \quad (5)$$

where R_s value was calculated via the formula: $R_s = U_{drop}/(2I_s)$.

According to a series-RC circuit model, the equivalent capacitances (C_{eq}, F g^{-1}) were calculated from alternating-current frequency response using the following equation [37,38]:

Table 1 The physical properties of CNF and BO-CNF-1, 2, 3, 4 films.

Sample	C (at%) (from XPS)	O (at%)	B (at%)	S_{BET} (m^2 g^{-1})	Film thickness (μm)	Packing density (g cm^{-3})
CNF	96.01	3.99	0	461.5	11.3±0.3	1.19±0.02
BO-CNF-1	93.57	5.36	1.08	568.9	13.0±0.3	1.01±0.02
BO-CNF-2	89.88	8.52	1.60	594.6	15.1±0.5	0.93±0.03
BO-CNF-3	90.02	8.01	1.97	613.5	24.8±1.7	0.60±0.05
BO-CNF-4	88.94	8.86	2.20	725.7	62.3±15.6	0.23±0.09

$$C_{eq} = \frac{-1}{2\pi f Z''} \cdot \frac{4}{2m} \quad (6)$$

where f (Hz) is frequency and Z'' is the imaginary part of the impedance.

Results and discussion

A schematic illustration of the synthesis route of BO-CNF films is shown in Scheme 1. First, we synthesized the carbonaceous nanofibers through a hydrothermal carbonization (HTC) method within a 1.6 L Teflon autoclave. The low and high magnification scanning electron microscopy (SEM) images reveal that the uniform carbonaceous nanofibers with smooth surface have an average diameter of about 80 nm (Figure 1a and the Supporting information Figure S1a). The carbonaceous nanofibers can be highly dispersed in ethanol because of the presence of oxygen-containing groups on the nanofiber surface [39]. Next, 1 mL boric acid ethanol solution was mixed with 4 mL (ca. 6 mg mL^{-1}) carbonaceous nanofibers to form a homogeneous suspension. After a simple casting and solvent-evaporation-induced self-assembly process [35,39], a brown paper-like composite film was fabricated. The size of the film can be arbitrarily extended with a larger Teflon substrate. Lastly, the film was carbonized at 800 °C for 2 h, leading to the generation of the BO-CNF film containing residual boric oxide. The boric oxide was dissolved in hot water to transform into boric acid, which could be used for cyclic utilization in the next boron doping. The final black film was mechanically robust and could be directly used as a free-standing electrode for the electrochemical measurements (Figure S2 and Scheme 1). In order to adjust the content of heteroatom doping, different masses of boric acid (0, 10, 20, 40, and 80 mg) were added, and the corresponding films were denoted as CNF and BO-CNF-1, 2, 3, 4 films, respectively.

The SEM images in Figure 1b-d and Figures S3 and S4 show the surface and cross-section of CNF and BO-CNF films. On account of the slight shrinkage after the decomposition of some oxygen-containing groups (such as -OH and -COOH) during the high temperature process, the diameter of carbonization nanofibers is decreased to about 70 nm (Figure S1b). The CNF, BO-CNF-1, and BO-CNF-2 films have a similar and flat surface morphology (Figure 1b and Figure S3). However, the BO-CNF-3, 4 films exhibit interconnected macropores with honeycomb-like structure, and the amount of honeycomb-like structure in BO-CNF-4 film (Figure 1c and d) is more than that in BO-CNF-3 film (Figure S3). We anticipate that the different surface structure is derived from the removal of excess boric oxide from the carbonization of composite films. Increased boric acid mass ratio blended in CNF film leaves more boric oxide crystal after carbonization, which generates more pores in the BO-CNT film after dissolving excess amount of boric oxide in hot water. The cross-sectional SEM images of CNF and BO-CNF-1, 2, 3, 4 films provide further information about the structure difference (Figure S4). The BO-CNF-3 and BO-CNF-4 films with obviously enlarged interspace are thicker than CNF, BO-CNF-1, and BO-CNF-2 films. Thus, the packing densities of CNF and BO-CNF-1, 2, 3, 4 films were calculated as 1.19 ± 0.02, 1.01 ± 0.02, 0.93 ± 0.03, 0.60 ± 0.05, and 0.23 ± 0.09 g cm^{-3}, respectively (Table 1), indicating lower packing density with increased boric acid content. Based on the sheet resistance and thickness of CNF and BO-CNF-1, 2, 3, 4 films, the electrical conductivities were calculated as 521, 403, 277, 114, and 35 S/m, respectively (Figure S2d).

X-ray photoelectron spectroscopy (XPS) was carried out to determine the surface chemical properties of CNF and BO-CNF samples. Figure 1e and Figure S5 present the detailed high-resolution XPS data of the B 1s and C 1s peaks with deconvolution. The XPS spectrum of the B 1s can be fitted into three peaks with binding energies of 189.5 eV (BC_3), 191.0 eV (BC_2O), and 192.3 eV (BCO_2) [33,40]. There are no peaks at 187-188 eV or at 193-194 eV, excluding the existence of B-B species and boric oxides, respectively [33]. Our BO-CNF-1, 2, 3, 4 samples show a significant boron content ranging from 1.08 to 2.20 at% (Table 1), which is higher than previously reported B-doped carbon materials (usually lower than 1 at%) [27,32,33]. For C 1s XPS spectra (Figure S5b), a main peak for C-C (at about 284.4 eV) and a minor peak for C-O (at 286 eV) can be easily distinguished. The oxygen content is increased from 3.99 to 8.86 at% as the boron content is increased (Table 1), which is consistent with the work reported by Cheng and may be due to the introduction of oxygen by boric acid [32].

Subsequently, we performed powder X-ray diffraction (XRD), Raman spectroscopy, and N_2 adsorption-desorption analysis to characterize the change of physical properties after heteroatom doping. The XRD patterns display that the CNF and BO-CNF samples have a pronounced and broad diffraction peak centered at 2θ of around 23° that can be assigned to graphitic carbon (Figure S6a), and no peaks could be assigned to boric oxide or boron carbide. From the CNF sample to BO-CNF-4 sample, the peak at 23° becomes weaker, indicating the gradual loss of long-range structural order of carbon. For all samples, two distinct peaks at 1330 and 1590 cm^{-1} in the Raman spectra (Figure S6b) can be assigned to the D and G bands of carbon, respectively. It is considered that the I_D/I_G value (relative intensity ratio of the D band to G band) is related to defects or disorder of carbon lattice [31,41]. Heteroatom doping introduces imperfections and defect sites into carbon lattice, inducing a high I_D/I_G value.

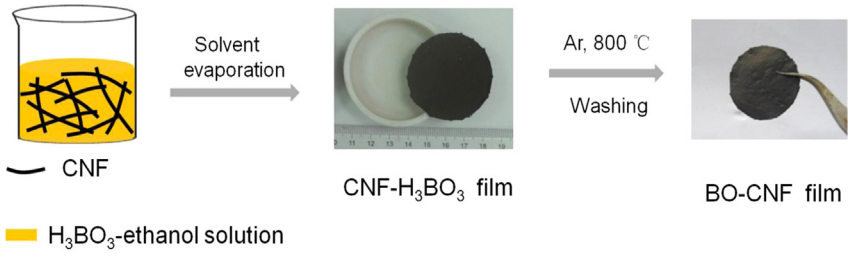

Scheme 1 A schematic to fabricate free-standing BO-CNF film.

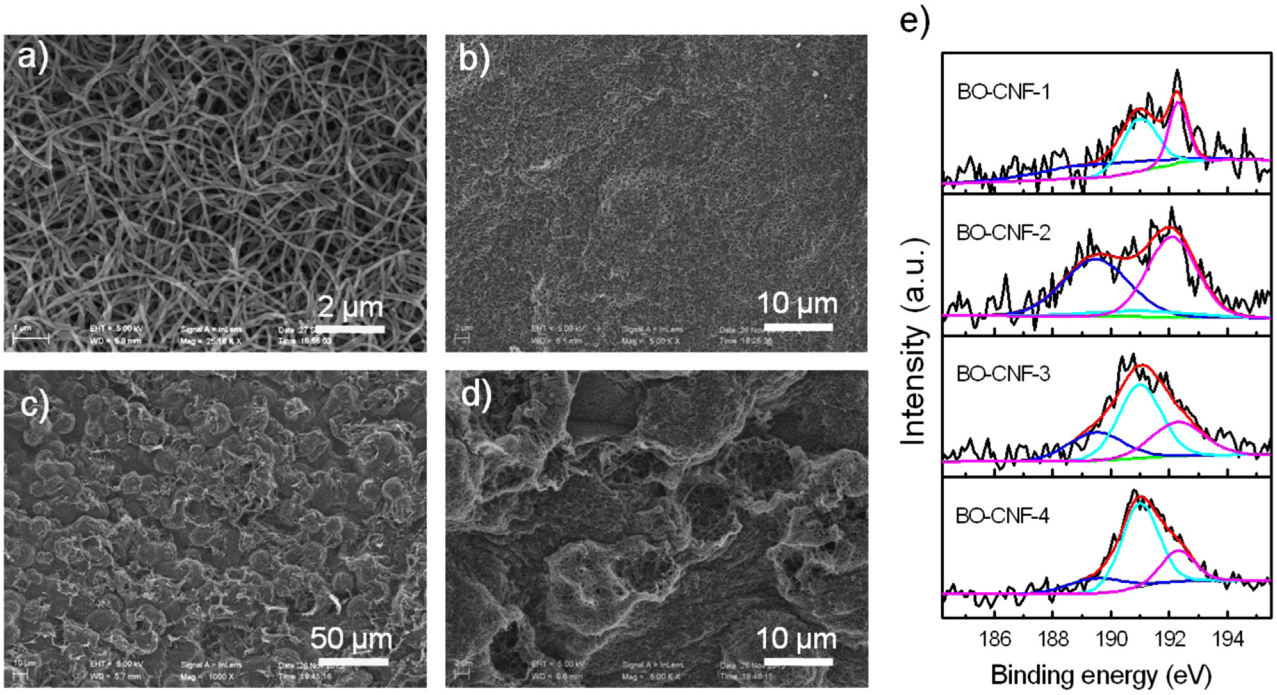

Figure 1 (a) SEM image of carbonaceous nanofibers fabricated by a HTC process. (b) SEM image of undoped CNF film after carbonization. (c) Low and (d) high magnification SEM images of the BO-CNF-4 film. (e) High-resolution B 1 s XPS spectra for BO-CNF-1, 2, 3, 4 samples.

The nitrogen isotherms of CNF and BO-CNF-1, 2, 3, 4 samples (Figure S7a) are characteristic for a microporous structure with type I sorption isotherm. The microporous structure is created by the evaporation of volatile species during the pyrolysis process [42]. The Brunauer–Emmett–Teller (BET) specific surface area (S_{BET}) is summarized in Table 1. A higher heteroatom content results in a larger S_{BET} value and the BO-CNF-4 sample demonstrates the largest S_{BET} of 725.7 $m^2\ g^{-1}$. In order to study the micropore structure (below 1 nm), CO_2 sorption was performed and the data was obtained based on a slit pore density functional theory model (Figure S7c and d) [9]. The cumulative pore volume is increased from CNF to BO-CNF-4 samples. The pore size distribution curves show the enhanced pore width after the doping, which is due to the etching process of carbon skeleton by boric acid during the high temperature carbonization [43]. All these results suggest that we have successfully prepared the BO-CNF films with adjustable heteroatom content, variable micropore structure and tunable packing density. The heteroatom might contribute to pseudocapcitance, and the increased micropore volume and pore size may be favored for ion adsorption so as to yield a high gravimetric capacitance. Meanwhile, the tunable packing density of the BO-CNF film provides an opportunity for optimizing the volumetric capacitance. Therefore, these features make our material system an interesting candidate to explore its potential for supercapacitor applications.

The electrochemical capacitive performances of our free-standing film electrodes (1.3-1.5 mg cm^{-2}, $1.0 \times 1.0\ cm^2$) without any binder or conductive agent were evaluated in 1.0 M H_2SO_4 aqueous electrolyte using a two-electrode configuration. We first performed cyclic voltammetry (CV) measurements and the typical CV curves at 50 mV s^{-1} for all different samples are showed in Figure 2a. The CNF film exhibits a nearly rectangular curve with a smaller CV integrated area compared to other BO-CNF films, while the CV curves of BO-CNF films are roughly rectangular in shape including a few humps because of the pseudocapacitive process [12]. The electrical double-layer (EDL) capacitance and the pseudocapacitance can be separated from the CV curve with the largest rectangle area and the remaining area, respectively (Figure S8) [44,45]. The EDL capacitance and the pseudocapacitance increased by 232% and 948% from CNF to BO-CNF-4, respectively, suggesting an increased electric charge storage capacity due to not only the effective specific surface area but also the heteroatom doping.

Further, it is well accepted that the galvanostatic charge-discharge test is a more reasonable method than CV test for determining the specific capacitance [6]. Hence, we carried out galvanostatic charge-discharge tests at various current densities in detail. The profiles of charge-discharge plots at current densities of 1 and 10 A g^{-1} (Figure 2b and Figure S8c) are almost linear and symmetrical, indicative of a high Coulombic efficiency. It can be observed that the discharge time is increased from CNF film to BO-CNF-4 film, which agrees with the observation of above CV tests. Figure 2c shows that the gravimetric capacitances of CNF and BO-CNF-1, 2, 3, 4 films at 1 A g^{-1} are 76.5, 159.5, 192.8, 204.3, and 225.9 F g^{-1}, respectively. The gravimetric capacitance value of BO-CNF-4 film is improved by a factor of about 3 compared to that of CNF. In addition, the gravimetric capacitance values are comparable with most of B-doped carbon and heteroatom-doped carbon nanofibers (see Supporting information Table S1).

As emphasized by Gogotsi et al. the volumetric performance is more significant than the gravimetric one in order to realize compact supercapacitor devices with high packing density [4,14]. Thus, the volumetric capacitance values are calculated by multiplying the gravimetric capacitances with the corresponding packing densities, and are plotted in

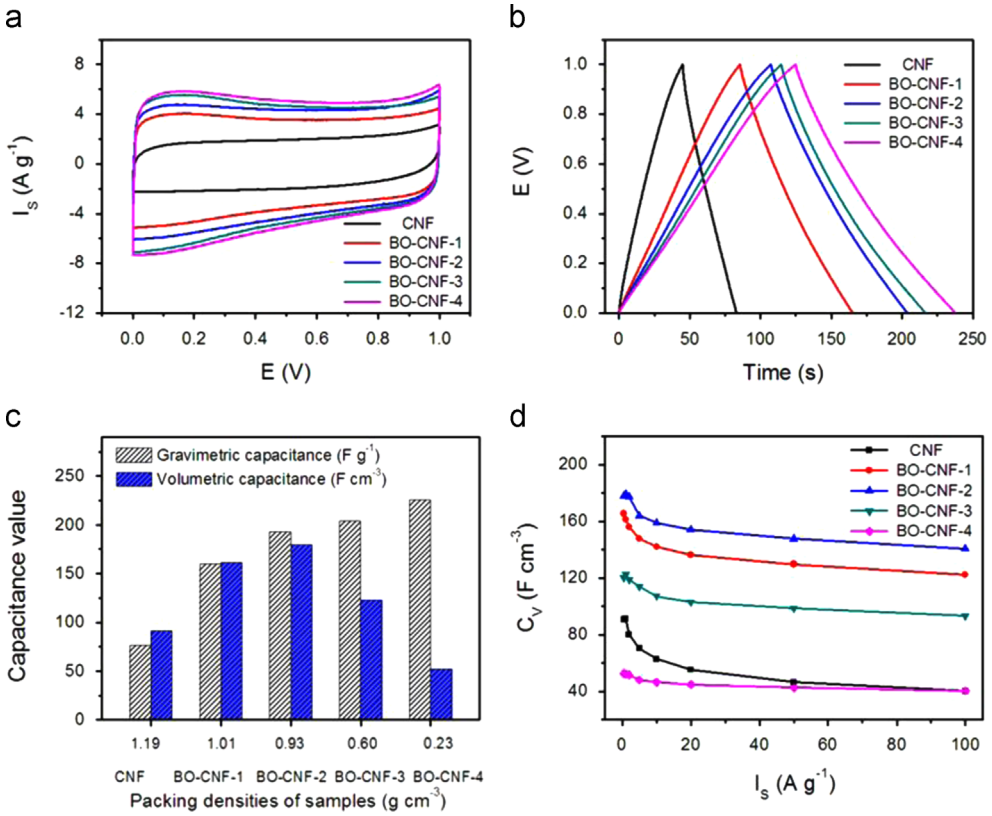

Figure 2 Electrochemical characterization of CNF and BO-CNF-1, 2, 3, 4 films in a two-electrode system. (a) CV curves at 50 mV s^{-1}, and (b) galvanostatic charge-discharge curves at 1 A g^{-1}. (c) Gravimetric and volumetric capacitances at 1 A g^{-1}. (d) Volumetric capacitances at different current densities.

Figure 2c. With the electrode ranging from CNF film to BO-CNF-2 film, the volumetric capacitance increases from 91.0 to 179.3 F cm^{-3} at a charge/discharge current density of 1 A g^{-1}, which is due to the strong increase of the gravimetric capacitance. However, because the packing density decreases rapidly from BO-CNF-2 film to BO-CNF-4 film in spite of the slight increase of gravimetric capacitance, the corresponding volumetric capacitance drops from 179.3 to 52.0 F cm^{-3}, showing a maxima volumetric capacitance of the BO-CNF-2 film (packing density of 0.93 g cm^{-3} and gravimetric capacitance of 192.8 F g^{-1}). Although many porous carbon materials, such as graphene foams and hydrogels/aerogels, exhibit a very high gravimetric capacitance, they have a low packing density and the void space of the carbon electrodes is flooded with electrolyte, increasing the weight of the whole device without improving capacitance value [4,14]. Therefore, the devices practically suffer from lower gravimetric performance and high volumetric performance with compact electrode design is highly needed for real device application. In our material system, the packing density is decreased from 1.19 to 0.23 g cm^{-3} while the gravimetric capacitance is increased from 76.5 to 225.9 F g^{-1} varying from CNF film to BO-CNF-4 film. The BO-CNF-2 film delivers the largest volumetric capacitance of 179.3 F cm^{-3} as well as maintains relatively high packing density and gravimetric capacitance (Figure 2c). Surprisingly, the BO-CNF-2 film retains a high volumetric capacitance of 158.9 F cm^{-3} and 140.7 F cm^{-3} at charge/discharge current densities of 10 and 100 A g^{-1}, respectively (Figure 2d), corresponding to a 78.5% capacitance retention with the working current densities increasing 2 orders of magnitudes. It is noteworthy that the volumetric capacitance values of our BO-CNF-2 film are among the best reported values of carbon-based materials so far (Table S2).

Rate capability is an important parameter to assess high-rate supercapacitors for fast charging/discharging application [46,47], so we attempt to explain the reason that accounts for such a remarkable rate capability of BO-CNF-2 film. For comparison, a powder electrode was prepared by adding 5 wt % poly-(vinylidene fluoride) (PVDF) binder to the BO-CNF-2 and the electrochemical performances were measured as the same method with film electrode. It can be seen from Figure 3a that the BO-CNF-2 film and powder electrodes show a similar charge-discharge characteristic at 1 A g^{-1}, while the difference of charge-discharge curves becomes pronounced at a high current density of 100 A g^{-1} (the inset), giving a shorter discharge time and a larger potential drop (U_{drop}) for the BO-CNF-2 powder sample. So the BO-CNF-2 powder exhibits a rate capability of 65.3% inferior to the BO-CNF-2 film (78.5%), but it is still better than CNF film with only 44.1% retention (Figure 3b).

Furthermore, these results can be explained by the electrochemical impedance spectroscopy (EIS) in Figure 3c and equivalent capacitances versus frequency response in Figure 3d. The equivalent series resistances of the CNF film, BO-CNF-2 film, and BO-CNF-2 powder electrodes are obtained from high-frequency region of Nyquist plots (the inset of Figure 3c) and are about 0.40, 0.43, and 0.48 Ω, respectively, which indicates that the addition of PVDF binder causes the deterioration of electrical conductivity and that the heteroatom doping has a small effect on

conductivity. In the low-frequency region, the BO-CNF-2 film exhibits the steepest slope of all samples, demonstrating an ideal capacitive behavior and the lowest electrolyte diffusion resistance. This can be attributed to the existence of continuous electrolyte ion transport channels, which were formed during the removal process of boric oxide by washing with hot water. Therefore, the BO-CNF-2 film with high electrical conductivity and efficient ion transport channel delivers the outstanding rate capability (larger than 75% retention from 1 to 100 A g^{-1}), exceeding most of other reported carbon-based powder electrodes and film electrodes (Table S3). At the meantime, it is worth mentioning that the capability retentions of other BO-CNF-1, 3, 4 films are 76.0%, 76.1%, and 77.3%, respectively (Figure 2d), close to that of BO-CNF-2 film, which also are reflected in the steep slope of Nyquist plots in the low-frequency region (Figure S9a). All BO-CNF films with excellent rate capability reveal that the ion diffusion network is retained in the compact films in despite of the absence of obvious macropores in the SEM images of B-CNF-1, 2 films. The equivalent capacitance values based on a series-RC circuit model (Figure 3d) also confirm that the B-CNF-2 film exhibits the slowest gravimetric capacitance loss over the entire frequency range.

The volumetric energy and power densities, as two key factors of the supercapacitor performance, are summarized in the Ragone plots based on the volume of electrode materials (Figure S9b). Among CNF and BO-CNF-1, 2, 3, 4 film electrodes, the BO-CNF-2 film demonstrates the highest volumetric energy density. The value of volumetric energy density is about 6.2 W h L^{-1} at a power density of 116.1 W L^{-1} and still maintains 3.8 W h L^{-1} at 20.5 kW L^{-1} (100 A g^{-1}). The maximum volumetric power density of as high as 197.0 kW L^{-1} was calculated from the U_{drop} against the current density (Figure S9c), and is much larger than those reported values [15,22,37,48]. In addition, the BO-CNF-2 film shows a good cycling stability with a capacitance loss of only 6.4% after 5000 cycles (Figure S9d).

Owing to the suitable platform provided by the BO-CNF film networks, a further enhancement of the supercapacitor performance can be obtained by loading other redox-based materials onto the network. As a proof of concept, polyaniline (PANI) with low cost and large pseudocapacitance was chosen [49,50]. The SEM images (inset of Figure 3e and Figure S10) show that PANI nanoparticles are uniformly anchored on the one-dimensional nanofibers, leading to a great increase in their capacitance values (Figure 3f and Figure S11). The BO-CNF-2@PANI film with an optimal PANI content delivers a volumetric (gravimetric) capacitance of 359.1 F cm^{-3} (278.4 F g^{-1}) at 1 A g^{-1}, which is much higher than that of BO-CNF-2 and CNF@PANI films. Figure 3f also shows a high rate capability of the BO-CNF-2@PANI film, indicating the incorporation of PANI without affecting the continuous electrolyte ion networks.

The above results present the outstanding volumetric performance and high rate capability of the synthesized BO-CNF film, which may be a promising electrode material. Nevertheless, for the practical commercial application, the cost of dopant must be taken into account since the synthesis of Te nanowires and carbon nanofibers can be easily scaled up by increasing the autoclave volume and the high-cost Te nanowires can be recycled with more than 80 wt% [51,52]. Despite boric acid has been widely utilized as boron source for B-doped carbon materials [32,41,43,53,54], the utilization ratio of boron atom is very low (see theSection 2). We considered boric acid

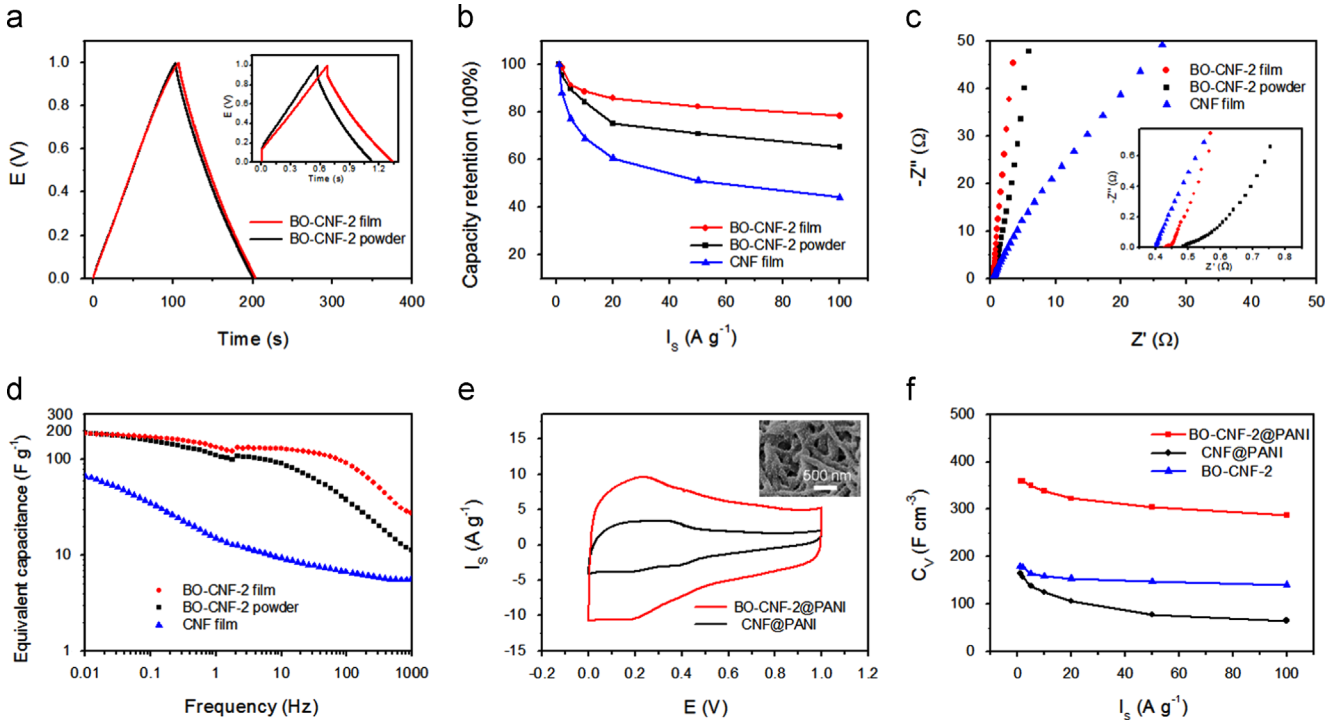

Figure 3 (a) Galvanostatic charge–discharge curves of BO-CNF-2 film and BO-CNF-2 powder (with 5% PVDF) at 1 A g^{-1} and 100 A g^{-1} (inset). (b) Capacity retentions at different current densities, (c) Nyquist plots, and (d) equivalent capacitances versus frequency response for three electrode materials. (e) CV curves at 50 mV s^{-1} for CNF@PANI and BO-CNF-2@PANI films. The inset is the SEM image of BO-CNF-2@PANI film. (f) Volumetric capacitances at different current densities for three samples.

recycle through a simple yet effective way by hot water washing, which yielded the boric acid with purity comparable to commercial ones confirmed by XRD measurement and a recovery ratio of approximately 50% (Figure S12). We also performed the electrochemical tests of BO-CNF-2 film prepared with the recycled boric acid. The CV and galvanostatic charge-discharge tests (Figure S12) show that no fading of capacitive performance is observed when using the recycled BO-CNF-2 film.

Conclusions

In summary, a new type of free-standing boron and oxygen co-doped carbon nanofiber film was prepared in a facile method, as the conductive agent- and binder-free electrode materials, which exhibited a balanced gravimetric capacitance and volumetric capacitance (192.8 F g^{-1} and 179.3 F cm^{-3} at 1 A g^{-1}), outstanding rate capability (78.5% capacitance retention with current density increasing from 1 to 100 A g^{-1}), and good cycling stability (93.6% retention after 5000 cycles). We suggest that a thin film structure with reasonable packing density in macroscale, a continuous interconnected network in microscale, and a finely tunable heteroatom doping in nanoscale are the keys to an improved electrochemical performance in multiple factors. In addition, an even higher volumetric capacitance (359.1 F cm^{-3} at 1 A g^{-1}) was obtained after depositing polyaniline on the BO-CNF film. The recycling of boron source was proven to be efficient and had no influence on the electrochemical performance. Hence, our heteroatom-doped carbon nanofiber film not only possesses great potential as high-performance supercapacitor material but also acts as an inspiration for finely tuning and designing electrode material structures to optimize supercapacitor performance.

Acknowledgments

This work is supported by the National Natural Science Foundation of China (Grants 21431006, 91227103), the Ministry of Science and Technology of the People's Republic China (Grants 2014CB931800, 2013CB933900), the Chinese Academy of Sciences (Grant KJZD-EW-M01-1), and Hainan Province Science and Technology Department (CXY20130046) for financial support. We thank Dr Zhen-Yu Wu, Jin-Long Wang for help with the synthesis of carbon nanofibers.

Appendix A. Supporting information

Supplementary data associated with this article can be found in the online version at http://dx.doi.org/10.1016/j.nanoen.2015.04.017.

References

[1] P. Simon, Y. Gogotsi, Nat. Mater. 7 (2008) 845–854.
[2] M.D. Stoller, S. Park, Y. Zhu, J. An, R.S. Ruoff, Nano Lett. 8 (2008) 3498–3502.
[3] Z.-S. Wu, Y. Sun, Y.-Z. Tan, S. Yang, X. Feng, K. Mullen, J. Am. Chem. Soc. 134 (2012) 19532–19535.
[4] P. Simon, Y. Gogotsi, Acc. Chem. Res. 46 (2012) 1094–1103.
[5] L. Hao, X. Li, L. Zhi, Adv. Mater. 25 (2013) 3899–3904.
[6] M.D. Stoller, R.S. Ruoff, Energy Environ. Sci. 3 (2010) 1294–1301.
[7] L.-F. Chen, Z.-H. Huang, H.-W. Liang, Q.-F. Guan, S.-H. Yu, Adv. Mater. 25 (2013) 4746–4752.
[8] A. Stein, Z. Wang, M.A. Fierke, Adv. Mater. 21 (2009) 265–293.
[9] Y. Zhu, S. Murali, M.D. Stoller, K.J. Ganesh, W. Cai, P.J. Ferreira, A. Pirkle, R.M. Wallace, K.A. Cychosz, M. Thommes, D. Su, E. A. Stach, R.S. Ruoff, Science 332 (2011) 1537–1541.
[10] L. Borchardt, M. Oschatz, S. Kaskel, Mater. Horiz. 1 (2014) 157–168.
[11] D. Hulicova-Jurcakova, M. Kodama, S. Shiraishi, H. Hatori, Z.H. Zhu, G.Q. Lu, Adv. Funct. Mater. 19 (2009) 1800–1809.
[12] L.-F. Chen, X.-D. Zhang, H.-W. Liang, M. Kong, Q.-F. Guan, P. Chen, Z.-Y. Wu, S.-H. Yu, Acs Nano 6 (2012) 7092–7102.
[13] Y. Xu, Z. Lin, X. Huang, Y. Wang, Y. Huang, X. Duan, Adv. Mater. 25 (2013) 5779–5784.
[14] Y. Gogotsi, P. Simon, Science 334 (2011) 917–918.
[15] M. Ghaffari, Y. Zhou, H. Xu, M. Lin, T.Y. Kim, R.S. Ruoff, Q.M. Zhang, Adv. Mater. 25 (2013) 4879–4885.
[16] N. Jung, S. Kwon, D. Lee, D.-M. Yoon, Y.M. Park, A. Benayad, J.-Y. Choi, J.S. Park, Adv. Mater. 25 (2013) 6854–6858.
[17] M.-Q. Zhao, C.E. Ren, Z. Ling, M.R. Lukatskaya, C. Zhang, K.L. Van Aken, M.W. Barsoum, Y. Gogotsi, Adv. Mater. 27 (2015) 339–345.
[18] Z. Ling, C.E. Ren, M.-Q. Zhao, J. Yang, J.M. Giammarco, J. Qiu, M.W. Barsoum, Y. Gogotsi, Proc. Natl. Acad. Sci. USA 111 (2014) 16676–16681.
[19] M. Ghidiu, M.R. Lukatskaya, M.-Q. Zhao, Y. Gogotsi, M. W. Barsoum, Nature 516 (2014) 78–81.
[20] M.R. Lukatskaya, O. Mashtalir, C.E. Ren, Y. Dall'agnese, P. Rozier, P.L. Taberna, M. Naguib, P. Simon, M.W. Barsoum, Y. Gogotsi, Science 341 (2013) 1502–1505.
[21] J. Benson, I. Kovalenko, S. Boukhalfa, D. Lashmore, M. Sanghadasa, G. Yushin, Adv. Mater. 25 (2013) 6625–6632.
[22] X. Yang, C. Cheng, Y. Wang, L. Qiu, D. Li, Science 341 (2013) 534–537.
[23] Y. Yoon, K. Lee, S. Kwon, S. Seo, H. Yoo, S. Kim, Y. Shin, Y. Park, D. Kim, J.-Y. Choi, H. Lee, Acs Nano 8 (2014) 4580–4590.
[24] D.N. Futaba, K. Hata, T. Yamada, T. Hiraoka, Y. Hayamizu, Y. Kakudate, O. Tanaike, H. Hatori, M. Yumura, S. Iijima, Nat. Mater. 5 (2006) 987–994.
[25] Y. Xu, Z. Lin, X. Zhong, X. Huang, N.O. Weiss, Y. Huang, X. Duan, Nat. Commun. 5 (2014) 4554.
[26] U.N. Maiti, W.J. Lee, J.M. Lee, Y. Oh, J.Y. Kim, J.E. Kim, J. Shim, T.H. Han, S.O. Kim, Adv. Mater. 26 (2014) 40–67.
[27] Z.-S. Wu, A. Winter, L. Chen, Y. Sun, A. Turchanin, X. Feng, K. Müllen, Adv. Mater. 24 (2012) 5130–5135.
[28] Z.-S. Wu, K. Parvez, A. Winter, H. Vieker, X. Liu, S. Han, A. Turchanin, X. Feng, K. Müllen, Adv. Mater. 26 (2014) 4552–4558.
[29] Z. Wen, X. Wang, S. Mao, Z. Bo, H. Kim, S. Cui, G. Lu, X. Feng, J. Chen, Adv. Mater. 24 (2012) 5610–5616.
[30] X. Zhuang, F. Zhang, D. Wu, X. Feng, Adv. Mater. 26 (2014) 3081–3086.
[31] L.-F. Chen, Z.-H. Huang, H.-W. Liang, W.-T. Yao, Z.-Y. Yu, S.-H. Yu, Energy Environ. Sci. 6 (2013) 3331–3338.
[32] D.-W. Wang, F. Li, Z.-G. Chen, G.Q. Lu, H.-M. Cheng, Chem. Mater. 20 (2008) 7195–7200.
[33] J. Han, L.L. Zhang, S. Lee, J. Oh, K.-S. Lee, J.R. Potts, J. Ji, X. Zhao, R.S. Ruoff, S. Park, Acs Nano 7 (2013) 19–26.
[34] Y. Fang, B. Luo, Y. Jia, X. Li, B. Wang, Q. Song, F. Kang, L. Zhi, Adv. Mater. 24 (2012) 6348–6355.
[35] H.-W. Liang, L. Wang, P.-Y. Chen, H.-T. Lin, L.-F. Chen, D. He, S.-H. Yu, Adv. Mater. 22 (2010) 4691–4695.
[36] H.-W. Liang, Q.-F. Guan, L.-F. Chen, Z. Zhu, W.-J. Zhang, S.-H. Yu, Angew. Chem. Int. Ed. 51 (2012) 5101–5105.

[37] X. Wang, Y. Zhang, C. Zhi, X. Wang, D. Tang, Y. Xu, Q. Weng, X. Jiang, M. Mitome, D. Golberg, Y. Bando, Nat. Commun. 4 (2013) 2905.
[38] J.R. Miller, R.A. Outlaw, B.C. Holloway, Science 329 (2010) 1637–1639.
[39] H.-W. Liang, X. Cao, W.-J. Zhang, H.-T. Lin, F. Zhou, L.-F. Chen, S.-H. Yu, Adv. Funct. Mater. 21 (2011) 3851–3858.
[40] L. Yang, S. Jiang, Y. Zhao, L. Zhu, S. Chen, X. Wang, Q. Wu, J. Ma, Y. Ma, Z. Hu, Angew. Chem. Int. Ed. 50 (2011) 7132–7135.
[41] Y. Zheng, Y. Jiao, L. Ge, M. Jaroniec, S.Z. Qiao, Angew. Chem. Int. Ed. 52 (2013) 3110–3116.
[42] Z.-Y. Wu, C. Li, H.-W. Liang, Y.-N. Zhang, X. Wang, J.-F. Chen, S.-H. Yu, Sci. Rep. 4 (2014) 4079.
[43] B.-H. Kim, K. Seung Yang, H.-G. Woo, Mater. Lett. 93 (2013) 190–193.
[44] Z. Lin, Y. Liu, Y. Yao, O.J. Hildreth, Z. Li, K. Moon, C.-p. Wong, J. Phys. Chem. C 115 (2011) 7120–7125.
[45] Y. Hu, H. Liu, Q. Ke, J. Wang, J. Mater. Chem. A 2 (2014) 11753–11758.
[46] Z. Bo, W. Zhu, W. Ma, Z. Wen, X. Shuai, J. Chen, J. Yan, Z. Wang, K. Cen, X. Feng, Adv. Mater. 25 (2013) 5799–5806.
[47] P. Simon, Y. Gogotsi, B. Dunn, Science 343 (2014) 1210–1211.
[48] M.F. El-Kady, V. Strong, S. Dubin, R.B. Kaner, Science 335 (2012) 1326–1330.
[49] D.-W. Wang, F. Li, J. Zhao, W. Ren, Z.-G. Chen, J. Tan, Z.-S. Wu, I. Gentle, G.Q. Lu, H.-M. Cheng, Acs Nano 3 (2009) 1745–1752.
[50] Y. Wang, X. Yang, L. Qiu, D. Li, Energy Environ. Sci. 6 (2013) 477–481.
[51] K. Wang, Y. Yang, H.-W. Liang, J.-W. Liu, S.-H. Yu, Mater. Horiz. 1 (2014) 338–343.
[52] J.-L. Wang, J.-W. Liu, B.-Z. Lu, Y.-R. Lu, J. Ge, Z.-Y. Wu, Z.-H. Wang, M.N. Arshad, S.-H. Yu, Chem. Eur. J. 21 (2015) 4935–4939.
[53] L. Niu, Z. Li, W. Hong, J. Sun, Z. Wang, L. Ma, J. Wang, S. Yang, Electrochim. Acta 108 (2013) 666–673.
[54] S. Wang, L. Zhang, Z. Xia, A. Roy, D.W. Chang, J.-B. Baek, L. Dai, Angew. Chem. Int. Ed. 51 (2012) 4209–4212.

Zi-You Yu received his Bachelor degree at Northeastern University in 2012, and now he pursues his Ph.D. in inorganic chemistry under the supervision of Professor Shu-Hong Yu at the University of Science and Technology of China (USTC). He is interested in synthesizing and designing carbon nanomaterials and metal molybdate/tungstate nanocomposites for energy conversion and storage.

Li-Feng Chen received his B.E. degree in 2006 from Anhui University of Technology and Ph.D. in chemistry under the supervision of Prof. Shu-Hong Yu at University of Science and Technology of China (USTC) in 2013. Then, he worked as a Postdoctoral Research Fellow with Prof. Shu-Hong Yu at USTC. His current research interests are carbon-based nanomaterials/nanostructures for efficient energy storage and conversion devices.

Lu-Ting Song received her Bachelor degree at Northeast Normal University in 2011, and now she pursues her Ph.D. in inorganic chemistry under the supervision of Professor Shu-Hong Yu at the University of Science and Technology of China (USTC). Her current research interests are three-dimensional carbon nanofiber hydrogels/aerogels and metal oxide nanocomposites for energy conversion and storage.

Yan-Wu Zhu joined University of Science and Technology of China in 2011 as a professor. He got his Ph.D. in condensed matter physics from National University of Singapore (2007). He was working as a postdoctoral fellow in the National University of Singapore Nanoscience & Nanotechnology Initiative (2007–2008) and in the Department of Mechanical Engineering at The University of Texas at Austin (2008–2011). He has co-authored more than 100 peer-reviewed papers. His current research includes carbon nanomaterials for efficient energy storage and conversion.

Heng-Xing Ji received his B.Sc. degree at University of Science and Technology of China (USTC) and his Ph.D. from the Institute of Chemistry, Chinese Academy of Sciences (ICCAS). He was working as a postdoctoral fellow in the Leibniz Institute for Solid State and Materials Research Dresden (2008–2013) and in the Department of Mechanical Engineering at The University of Texas at Austin (2010–2013). He joined USTC in 2013 as a professor. His current research includes the size effect and the surface/interface effect of low-dimensional carbon nanostructures in the efficient energy storage devices, and the design of novel carbon nanomaterials.

Shu-Hong Yu received his B.Sc. degree at Hefei University of Technology and his Ph.D. from the University of Science and Technology of China (USTC). After he finished Postdoctoral research in the Tokyo Institute of Technology and the Max Planck Institute of Colloids and Interfaces, he was appointed as a full professor in 2002 at the USTC, and was awarded the Cheung Kong Professorship. He research interests include design and synthesis, and self-assembly of new nanostructured materials and composite materials, and their applications for energy conversion, catalysts, and nanodevices. He serves as an editorial advisory board member of journals *Accounts of Chemical Research, Chemical Science, Materials Horizons, Chemistry of Materials, Nano Research, CrystEngComm, Particle and Particle Systems Characterisation* and *Current Nanoscience*. His recent awards include *Chemical Soc. Rev. Emerging Investigator Award* (2010) and *Roy-Somiya Medal of the International Solvothermal and Hydrothermal Association* (ISHA) (2010).